Check for updates

Synthesis of graphene derivatives from asphaltenes and effect of carbonization temperature on their structural parameters

Faisal S. AlHumaidan, [ID] * Mohan S. Rana, [ID] Mari Vinoba, [ID] Hanadi M. AlSheeha, Afnan A. Ali and R. Navvamani

A method for synthesizing graphene derivatives from asphaltene is proposed in this work. The graphene derivatives are mainly composed of few-layer graphene-like nano-sheets of randomly distributed heteroatoms; mainly sulfur and nitrogen. The proposed method is based on a thermal treatment in which asphaltene is carbonized in a rotating quartz-tube furnace under an inert atmosphere at a temperature in the range of 400–950 °C. Asphaltenes from different origins were employed to verify the synthesis method. The results indicate that graphene derivatives obtained at high carbonization temperature have similar structural parameters, despite the evident differences in parent asphaltenes structures and compositions. The transformation of asphaltene to graphene derivatives mainly occurred due to three factors: the reduction in the average number of aromatic layers (n), the expansion in aromatic sheet diameter (L_a), and the elimination of alkyl side chains. The reduction in the number of aromatic sheets per stack is primarily ascribed to thermal exfoliation, while the increase in the aromatic sheet diameter is attributed to secondary reactions in the aromatic core of asphaltene. The elimination of side chains, on the other hand, is mainly credited to thermal cracking. The quantification of defect density (L_D) in the graphene derivatives suggests an association between defects and heteroatoms presence.

Introduction

Crude oil mainly consists of four hydrocarbon fractions: saturates, aromatics, resins, and asphaltenes (SARA fractions). Asphaltene is regarded as the fraction of crude that is soluble in aromatic solvents, but insoluble in light paraffins (*i.e.*, hexane and heptane). The hypothetical structure of asphaltene suggests that it is composed of a highly condensed polycyclic aromatic core substituted with alkyl side chains, with traces of heteroatoms (*e.g.*, S, N, and O) and traces of metals (*e.g.*, Ni and V) as part of its ring system. The aromatic core of asphaltene is composed of stacked aromatic sheets, and the number of these sheets per stack may vary between the different asphaltene molecules (*i.e.*, 3–8 sheets per stack). Each sheet normally has 3–10 rings, mostly aromatic, but not excluding naphthenic and non-aromatic cyclic rings. The interlayer distance between the sheets normally remains in the range of 0.35–0.36 nm. Thus, asphaltene can be viewed as a layered material that has a similar structure to few-layer graphene hydrocarbon materials.[1]

Asphaltene is often viewed as a low-value byproduct in the petroleum industry, or sometimes a waste, due to its economic burdens. However, such inferior classification can be changed

by transforming the asphaltene into attractive products, such as graphene derivatives. The term graphene derivative in this work refers to a few-layer graphene-like nano-sheets of randomly distributed heteroatoms (*i.e.*, sulfur and nitrogen). The transformation of asphaltene into graphene derivative is potentially possible since the core of asphaltene is mainly composed of layered aromatic structure.[1] The transformation of asphaltene to graphene and its derivatives has been investigated by a number of research groups. Some research groups employed the chemical vapour deposition (CVD) to synthesize multi-layer graphene from asphaltene,[2–5] while other research groups utilized the liquid adsorption approach.[6,7] Chemical treatments were also employed to synthesize graphene derivatives from asphaltene.[8,9] Likewise, the thermal approach was attempted to synthesize graphene derivative from asphaltene.[9,10] The recent trend in research clearly reveal that such synthesized carbon materials have expanding industrial applications in energy storage,[11] sensor development,[12] and thermal management.[13,14]

This study is a continuation to our previous effort, in which we have synthesized few-layer carbon material from asphaltene by thermal treatment.[9,10] In this work, we have further extended our previous research to provide a thermal treatment method that can synthesis graphene derivatives, similar to sulfur/ nitrogen co-doped few layer graphene, from different asphaltene samples. The asphaltene samples have been selected from

Petroleum Research Center, Kuwait Institute for Scientific Research, Kuwait. E-mail: fhumaidan@kisr.edu.kw

different origins to ensure the diversification in structures and compositions. The results confirmed that the proposed carbonization method is very effective in converting the different asphaltene samples to few-layer graphene derivatives, especially at high carbonization temperature (*i.e.*, 950 °C). The graphene derivatives formed at high carbonization temperature illustrated very comparable structures, despite the differences in the parent asphaltenes structures and compositions. This study also confirmed that the observed defects in the aromatic sheets are mainly attributed to the presence of heteroatoms.

Experimental

Asphaltene separation

The asphaltene samples were extracted from three crude oils; namely, Kuwait export crude (KEC), Lower-Fars heavy crude (LF), and Mexican Ku-crude oil (Ku). KEC is a conventional crude oil while LF and Ku are heavy crude oils. KEC and LF asphaltenes belong to same region (Kuwait), yet, their compositions and structures are not similar. Our previous studies on Kuwaiti asphaltenes clearly indicated that LF-asphaltene is comparatively larger than the other asphaltenes and has relatively more heteroatoms, yet, it is more prone and susceptible to structural changes when exposed to thermal treatment.[1,15] Ku-asphaltene, on the other hand, is known for its high hetero-atom and metal contents, which can provide good information about the impact of precursor's impurities (*i.e.*, Ni, V, S, and N) on the properties of carbonized products. The asphaltenes were extracted in accordance with the method described in IP 143/90 standard (ASTM 6560), using *n*-heptane solvent extraction in a ratio of 30 ml to each 1 gm of sample. The compositions of the extracted asphaltenes are shown in Table 1.

Thermal treatment

The thermal treatment in this study was performed in both a stationary-tube furnace and a rotating quartz-tube furnace.[9] The carbonized products from the stationary furnace were inhomogeneous with significant amount of ash, while the ones obtained from the rotating furnace were homogeneous without any traces of ash. Therefore, the rotating quartz-tube furnace was adopted for the carbonization of asphaltene. In each run, approximately 4 g of asphaltene was carbonized in the quartz-tube, where the process was started by increasing the temperature at a rate of 3 °C min^{-1}, until reaching the set point (*i.e.*, 400–950 °C). The sample then remained at the carbonization temperature for about 4 h. To prevent oxidation reactions, an inert medium was maintained in the reaction zone throughout the whole carbonization process by introducing a stream of nitrogen at a flow rate of 300 ml min^{-1}. To ensure a uniform heat exposure on all asphaltene particles, the furnace was continuously turning in a rotation angle of 360° at an oscillation frequency of 3 rotations per minute in each direction. The weight losses due to the thermal treatment fell in the range of 49–55%.

Product characterization

The quality of the carbonized product has been verified by different characterization methods, which include the X-ray Diffraction (XRD), Raman Spectroscopy, Fourier-Transform Infrared Spectroscopy (FTIR), Transmission Electron Microscopy (TEM), Scanning Electron Microscopy (SEM), Energy Dispersive Spectroscopy (EDS), and carbon, hydrogen, nitrogen, sulfur CHNS elemental analysis.

The XRD analysis was employed in this study to determine the crystallinity level and monitor the changes in structural parameters with thermal treatments. The analysis was performed on the powdered samples using a high-power X-ray diffractometer (X Pert PRO, PANalytical XRD). The diffraction patterns ($2\theta = 6$–$90°$) were recorded at room temperature using Cu Kα radiation ($\lambda = 1.54055$ Å) at a scanning speed of 30 min^{-1} and step size of 0.02 (2θ). Each scan was conducted twice, and the recorded patterns were de-convoluted to precisely determine the peak position, peak intensity, peak area, and the full width at half maximum (FWHM). The FTIR analysis was also used to identify the surface functional group in the parent asphaltene and to investigate the changes in these functional groups after the thermal treatments. The analysis was performed in FTIR Spectrometer (Vertex 70, Bruker), where the spectra were recorded between 4400 and 400 cm^{-1} by performing collective 32 scans with baseline corrections. In FTIR analysis, the analytical chamber was kept under N$_2$ atmosphere (50 L h^{-1}), and pellets were prepared by diluting the sample with KBr (1 : 200).

Raman Spectroscopy was also utilized to characterize the parent asphaltene and its carbonized products. The analysis was performed on a BRUKER SENTERRA RamanScope III, equipped with Olympus trinocular head with a video camera. The images were transferred to OPUS 7.0 software and visualized within the OPUS video display of the connected PC. The Raman scattered light was analyzed by a double monochromator and was detected by a photomultiplier tube. Before conducting the Raman analysis, the samples were milled in a mortar to reduce their particle sizes. A small quantity of

Table 1 Compositions of asphaltenes

Elements	Normalized asphaltene content, wt%		
	KEC	LF	KU
C	82.29	80.05	82.50
H	8.31	8.04	8.12
S	8.28	10.69	7.56
N	0.83	0.38	1.07
Al	0.01	—	0.01
Mg	—	0.02	—
Si	0.23	0.21	0.01
Cl	0.01	0.12	0.07
K	0.05	0.04	0.04
Ca	—	0.09	0.01
V	—	0.16	0.45
Fe	—	0.13	0.02
Ni	—	0.05	0.10
Br	—	0.01	0.01
P	—	—	0.01
Total	100	100	100

RSC Advances

Paper

a mortared sample was placed on the sample holder and its surface was manually flattened under the microscope. A visually acceptable flat area was chosen as the focal point for laser excitation, and a series of spectra and acquisitions were performed. All Raman spectra were recorded using an excitation wavelength (λ) of 532 nm (excitation energy $E_l = 2.33$ eV), with a Laser power of 5 mW as the radiation source. The spectral resolution in the Raman shift was ranging from 50 to 4500 cm^{-1}.

The CHNS elemental analysis has been also utilized to determine the composition of the major elements in the asphaltene and its carbonized products. The CHNS analysis was conducted by an automated elemental analyzer, LECO-CHNS 628S (S add-on model). The reported results were the average of three test runs. SEM with EDS has been also utilized to verify the elemental composition and monitor the surface morphology. The SEM analysis was performed on a JEOL JEM-IT300 with Oxford instrumentation energy dispersive system. The samples were mounted on aluminium holders with carbon adhesive tape, and were coated with gold. The condition of analysis was 20 kV, and high vacuum was used. The images were taken with secondary electron detector. The elemental composition was analyzed by EDS (Oxford-Xmax20) using Aztec software. Furthermore, high-resolution TEM has been employed to provide further insight into the micro-structures and to verify the crystalline parameters that were previously measured by the XRD and Raman spectroscopy. The TEM microstructural examination was performed by a JEOL JEM-2100 transmission electron microscope at an accelerating voltage of 200 kV. Before analysis, the samples were powdered in an agate mortar and then ultrasonically dispersed in ethanol. A drop of this solid/liquid dispersion was placed on the Lacey Formvar/Carbon coated Cu grid. The TEM images were analyzed by the industry standard software for TEM experimental control and analysis, which is Digital-Micrograph software.

Results and discussion

Asphaltene is characteristically considered as a macro-molecule of rigid aromatic core with flexible alkyl side chains and relatively high amount of heteroatoms and metals. Asphaltene can be regarded as an ideal template to form few-layer graphene-like carbon nano-sheets since its aromatic moieties can be rearranged to form such structure. Different asphaltenes have been transformed in this study to few-layer graphene derivatives using different methods of thermal treatment. The most effective method was the carbonization in a rotating quartz-tube furnace under inert atmosphere at a controlled heating rate, which resulted in an efficient homogeneous carbonization. The carbonized products were thoroughly analyzed using different characterization techniques to determine their structural parameters and to verify the formation of graphene derivatives.

Characterization of structural parameters

The impact of thermal treatment in this study is revealed by comparing the macro-structures of parent asphaltenes with their corresponding carbonized products, which were obtained at different temperatures. Many structural parameters have been measured, including the layer distance between the aromatic sheets (d_m), the distance between aliphatic chains and naphthenic sheets (d_γ), the average diameter of the aromatic
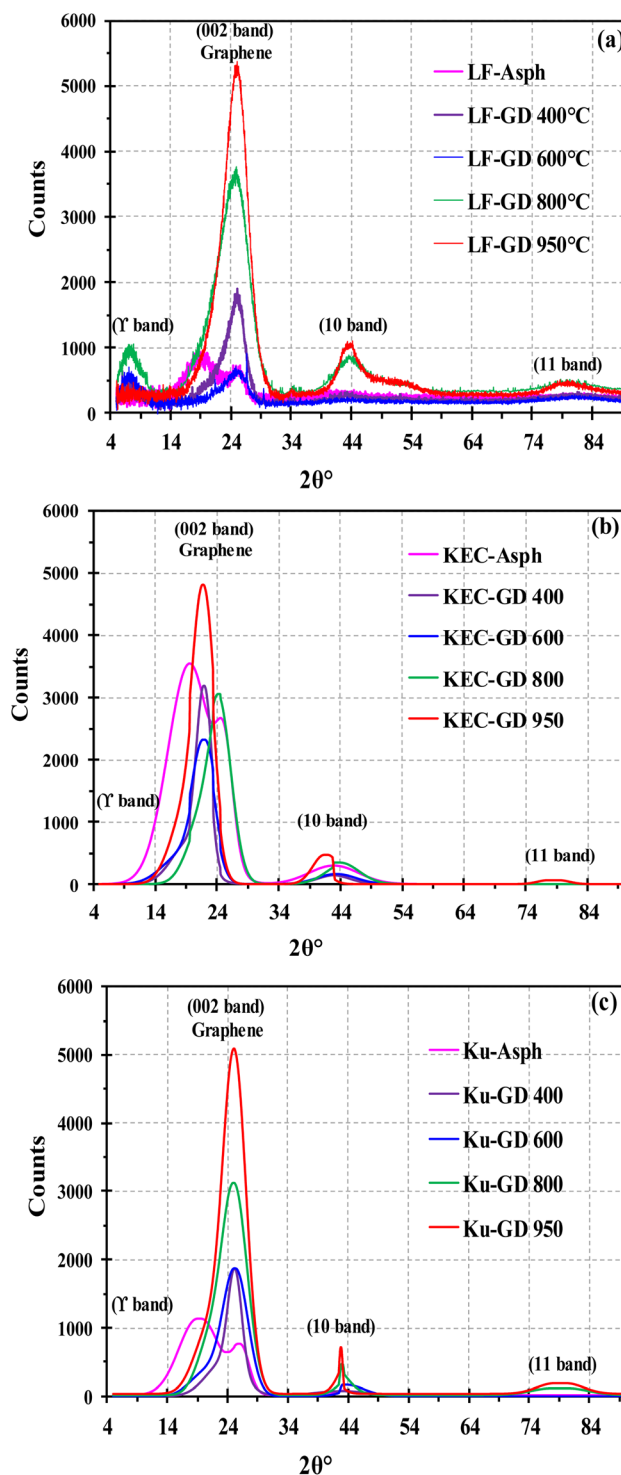

Fig. 1 Baseline corrected XRD patterns for the three asphaltenes along with their corresponding graphene derivatives at different temperatures: (a) LF, (b) KEC and (c) Ku.

Table 2 Structural parameters derived from XRD analysis for LF-asphaltene and its corresponding graphene derivative

Sample	d_m (Å)	d_γ (Å)	L_a (Å)	L_c (Å)	n	NO_{ar}	f_a
LF-asph.	3.6	5.8	11.7	22.7	7.4	4.4	0.17
LF-GD-400	3.6	5.1	9.4	24.8	8.8	3.5	0.72
LF-GD-600	3.6	5.2	16.5	19.3	6.4	6.2	0.81
LF-GD-800	3.6	5.3	25.4	15.9	5.4	9.5	0.78
LF-GD-950	3.5	5.1	37.9	18.3	6.2	14.2	0.78

Table 3 Structural parameters derived from XRD analysis for KEC-asphaltene and its corresponding graphene derivative

Sample	d_m (Å)	d_γ (Å)	L_a (Å)	L_c (Å)	n	NO_{ar}	f_a
KEC-asph.	3.5	5.7	17.3	24.7	8	6.5	0.15
KEC-GD 400	3.5	4.9	25.1	27.9	8.9	9.4	0.62
KEC-GD 600	3.5	5.2	22.1	18.1	6.1	8.3	0.72
KEC-GD 800	3.6	5.3	22.7	16.9	5.8	8.5	0.75
KEC-GD 950	3.5	5.2	36.9	18.3	6.2	13.8	0.78

Table 4 Structural parameters derived from XRD analysis for Ku-asphaltene and its corresponding graphene derivative

Sample	d_m (Å)	d_γ (Å)	L_a (Å)	L_c (Å)	n	NO_{ar}	f_a
Ku-asph.	3.6	5.9	20.8	26.1	8.4	7.8	0.18
Ku-GD 400	3.5	4.7	14.2	29.8	9.4	5.3	0.52
Ku-GD 600	3.6	5.5	22.7	16.9	5.8	8.5	0.81
Ku-GD 800	3.6	5.4	27.6	15.9	5.5	10.3	0.85
Ku-GD 950	3.6	5.4	36.7	17.4	5.9	13.7	0.83

sheet (L_a), the cluster diameter (L_c), the number of aromatic sheet per stack (n), the average number of aromatic ring per sheet (NO_{ar}), and the aromaticity (f_a). The results clearly revealed that the transformation of asphaltene molecules into graphene derivatives are mainly ascribed to three factors: the elimination of the alkyl side chains, the reduction in the number of aromatic sheet per stack (n), and the increase in the aromatic sheet diameter (L_a). The elimination of the alkyl side chains from the asphaltene core is mainly caused by thermal cracking reactions, whereas the reduction in the number of aromatic sheets per stack resulted from thermal exfoliation. The increase in aromatic sheet diameter, on the other hand, is primarily associated with the secondary reactions in the aromatic core.

The structural parameters of the parent asphaltenes and their corresponding carbonized products have been measured by XRD. Fig. 1 illustrates the baseline corrected XRD patterns for the three parent asphaltenes and their corresponding graphene derivatives at different carbonization temperatures. The change in crystallinity level with temperature is clearly reflected by the strong peak observed at $2\theta = 26°$, which is known as the graphene band. The XRD patterns in Fig. 1 also shows the four characteristic bands (i.e., γ, graphene, 10, and 11) from which the structural parameters of crystalline carbon materials were measured.[1,16,17] Tables 2–4 illustrate the structural parameters

from the XRD analysis for the three asphaltenes along with their corresponding graphene derivatives. The results clearly designate that the layer distance between the aromatic sheets (d_m) and the distance between aliphatic chains and naphthenic sheets (d_γ) are not considerably affected by the severity of thermal treatment. The average distance between the aromatic layers in the parent asphaltenes was about 3.6 Å, and almost remained constant at all carbonization temperatures. The distance between aliphatic chains and naphthenic sheets, on the other hand, has slightly decreased by less than 1.0 Å. Conversely, the average diameter of aromatic sheet (L_a) has significantly increased with thermal treatment severity. The results also revealed notable reductions in the cluster diameter (L_c) and the number of aromatic sheets per stack (n) as the carbonization temperature increases. As previously stated, the observed changes in the structure of asphaltenes, which transform them into few-layer graphene-like materials, mainly occur through three mechanisms: the reduction in aromatic sheet number per stack, the expansion in aromatic sheet diameter, and the elimination of alkyl side chains. These three mechanisms are further discussed in the following sections.

Reduction in the number of aromatic sheets

The structural parameters obtained from XRD revealed obvious reduction in the number of aromatic sheet (n) per stack as the carbonization temperature increases. The decrease in the number of aromatic sheet was also associated with a notable reduction in the cluster diameter or the stack height (L_c). The observed reductions in these structural parameters are primarily caused by thermal exfoliation. The measurements of the stack height and the number of aromatic sheet per stack in the carbonized products clearly infers the formation of few-layer carbon materials, since the thickness of a single carbon layer is approximately 3.4 Å. One of the observation that can be noted in the XRD measurements for the three sets of samples is the slight increase in the number of aromatic sheet per stack at mild carbonization temperature (i.e., 400 °C), which is followed by a notable decrease in this structural parameter as the carbonization temperature increases. This initial increase can be attributed to the removal of the alkyl side chains, which facilitated the stacking of the aromatic sheet. However, the further increase in carbonization temperature enhances the thermal exfoliation, which resulted in a decrease in the number of aromatic sheets per stack. The thermal exfoliation in this study can be attributed to the weakening of the van der Waals interactions between layers, caused by heteroatoms functionalities.[18] Poh et al.[18] reported similar thermal exfoliation for graphite oxide in an inert gas (i.e., N_2) and in sulfur-containing gases (i.e., H_2S, CS_2, and SO_2) at a temperature range of 600–1000 °C. The study revealed that exfoliation in sulfur gaseous environment resulted in the inclusion of more heteroatoms on the graphene surfaces as compared to nitrogen gaseous environment. The amount of sulfur reported by Poh and coworkers in the S-doped graphene was in the range of 4–12 wt%, which is comparable to the one observed in the graphene derivatives of this study (8–11 wt%), as will be later shown. In addition to
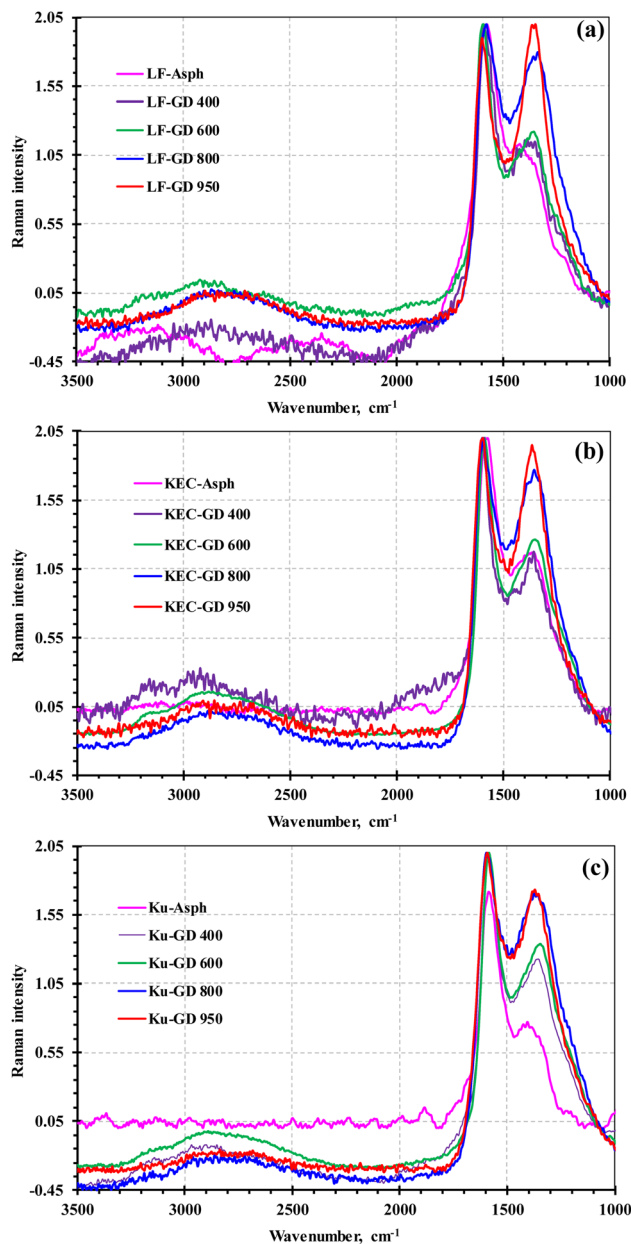
Fig. 2 Raman spectra of the three asphaltenes and their corresponding graphene derivatives at different temperatures: (a) LF, (b) KEC and (c) Ku.

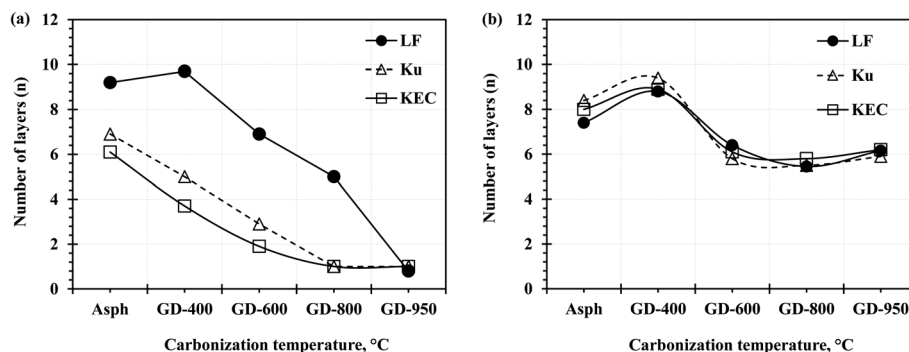heteroatom functionalities, the thermal exfoliation in asphaltene core can be ascribed to the decomposition of metalloporphyrin structures (Ni and V complexes in asphaltene), which significantly affect the π-electronic interaction between layers.[19]

To further verify the XRD finding, the Raman analysis was employed. The Raman spectra of the parent asphaltenes and their corresponding graphene derivatives are illustrated in Fig. 2. The Raman spectra clearly reveal the formation of crystalline carbon materials, which is shown by the two prominent peaks at ~1350 and ~1580, respectively known as the D and G. The D band is mainly associated with defects and disorder in the graphitic structure, including the grain boundaries and heteroatoms; whereas the G band corresponds to the in-plane vibration of the sp^2 carbon. The calculation of structural parameters of carbon-based material from Raman spectra is a subject of dispute and discrepancy in literature;[20] yet, there is agreement among researchers that the intensity ratio between the D- and G-bands (I_D/I_G) and the full width at half maximum of the G-band ($FWHM_G$) are the two main graphitization indicators in Raman analysis. The literature also indicates that the changes in the number of aromatic layer in crystalline carbon materials is closely associated with the G-band position, where an increase in layers is normally reflected by a 3–5 cm^{-1} shift toward lower wavenumber in the G-band position.[21–25] Therefore, the G-band position is commonly reported at 1581.6 for graphite ($n = \infty$), while it is detected at 1587 cm^{-1} for monolayer graphene ($n = 1$). Based on these findings, empirical equations have been proposed to determine the number of layers in graphene and graphene-like materials from the G-band position.[22,25] Some literature also indicated that the 2D band can be employed in determining the number of aromatic layer through the relative intensity of I_{2D}/I_G.[21–24] This band arises due to a second-order two-phonon process and often reported at ~2630–2700 cm^{-1} in carbon allotropes. Yet, there is almost an agreement in literature that the utilization of the 2D band in measuring the number of layers is rather complex because the band is composed of several overlapping peaks, which make the 2D band in multi-layer graphene undistinguishable from that of graphite. Therefore, the number of aromatic sheet per stack in this study was measured from the G-band position.[22,25]

Fig. 3 compares the Raman and XRD measurements for the number of aromatic sheet per stack for the three asphaltenes

Fig. 3 The number of aromatic sheet per stack (*n*) for the parent asphaltenes and their corresponding graphene derivatives (a) Raman results (b) XRD results.

and their graphene derivatives. Both measurements confirm the thermal exfoliation, observed by the reduction in the number of aromatic sheets per stack, but it is more evident in the Raman

measurement. It is important to note here that the Raman measurements are very sensitive to the G-band position; hence, the first-order region in Raman spectrum was fitted with only
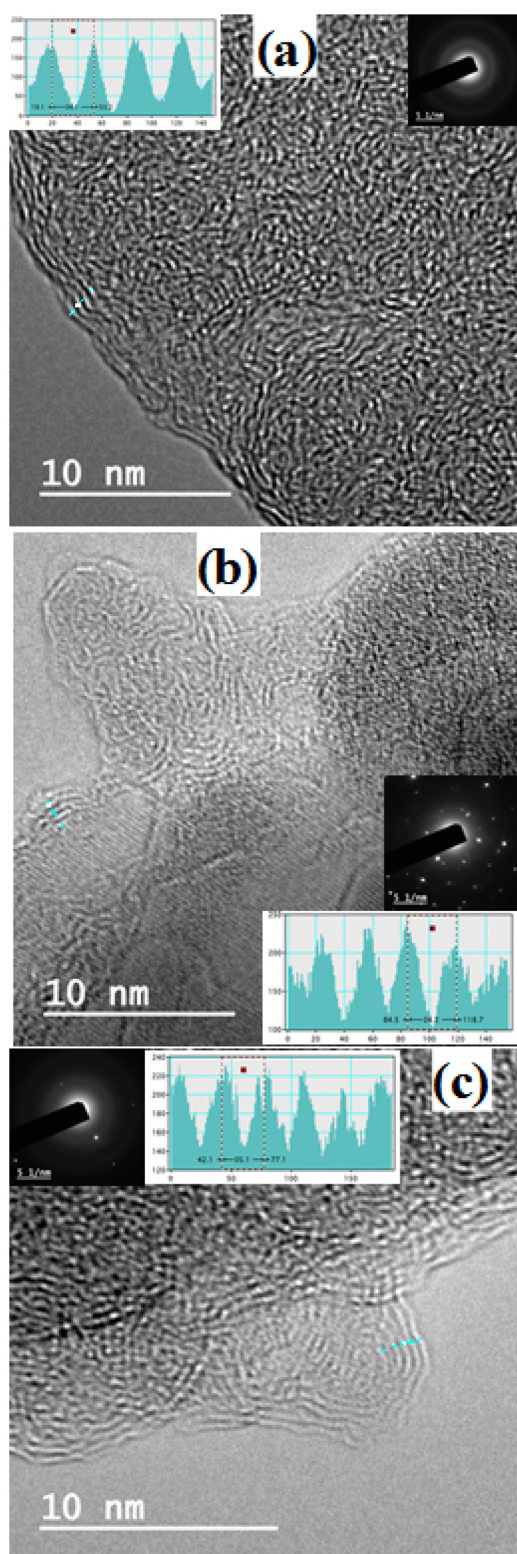

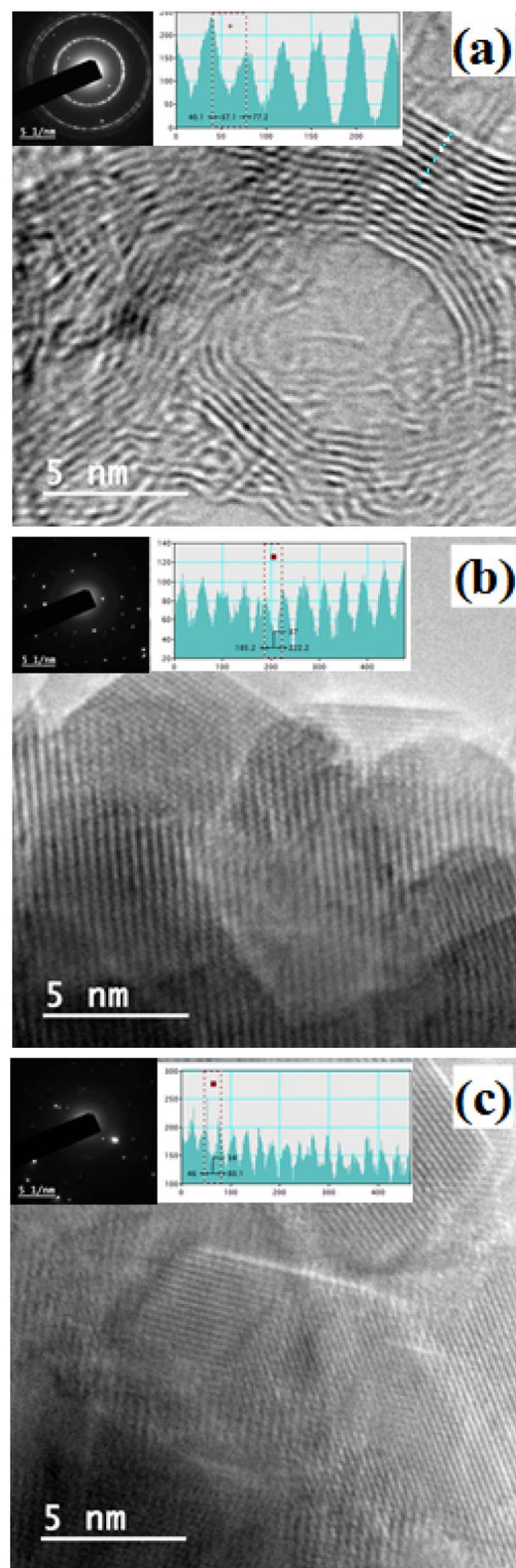Fig. 4   TEM analysis of the three parent asphaltenes; (a) LF, (b) KEC and (c) Ku.

Fig. 5   TEM analysis of graphene derivatives; (a) Ku-GD 800, (b) KEC-GD 800 and (c) Ku-GD 950.

two peaks (*i.e.*, G- and D-bands) using the Gaussian function, as recommended by AlHumaidan and Rana.[20] Fitting the spectrum with more peaks results in splitting the G-band into two bands (*i.e.*, G and D2-bands), and consequently prevents the utilization of Raman in such measurement.

The reduction in the number of aromatic layers through thermal exfoliation has been also confirmed by the high-resolution TEM. Fig. 4 illustrates the agglomerations of parent asphaltenes, where tangled structures with edges similar to cauliflower are observed. Such tangled structures are mainly ascribed to the presence of alkyl side chains, which impede the aromatic sheet from stacking.[26] The poor stacking of aromatic sheets can be observed everywhere in the asphaltene aggregates. The TEM results also reveal that the average number of aromatic sheet per stack for all parent asphaltenes is approximately 5. These results are quite comparable with the previously reported XRD and Raman results. Furthermore, the TEM analysis also indicates that the inter-layer distance between the neighbouring aromatic layers (d_m) in the parent asphaltene falls in the range of 0.34–0.36 nm (3.4–3.6 Å), which is in agreement with the XRD findings (~3.6 Å). Fig. 5, on the other hand, exemplifies the TEM results of the graphene derivatives obtained at severe carbonization temperatures (800–950 °C). The results clearly designate that the tangled structure has nearly disappeared after severe thermal treatment, which can be primarily attributed to the removal of the alkyl side chains. The proper stacking in Fig. 5 also implies that the average number of aromatic sheet per stack in the carbonized product has significantly decreased and might be in the range of 1–2, which is in agreement with the Raman results (Fig. 3a). The histograms in Fig. 5 also show that the distance between the neighbouring aromatic sheet has slightly increase from ~0.34 in parent asphaltenes to around ~0.37 nm. Both the decrease in the number of aromatic sheet per stack and the slight increase in the interlayer distance between layers endorse the previous conclusion about the thermal exfoliation.

Expansion in the aromatic sheet diameter

The XRD results; in Tables 2–4; also illustrate an evident increase in the average diameter of aromatic sheet as the carbonization temperature increases. In fact, at relatively mild carbonization temperature (*i.e.*, 400 °C), the size of L_a slightly decreased, and this can be associated with the removal of the alkyl side chains. However, significant increases were observed in L_a for all samples at higher temperatures. The increase in L_a would suggest that the aromatic core has undergone secondary reactions, such as cyclization of alkyl side chains, combination of rings radicals by polymerization, dehydrogenation of naphthenic rings (aromatization), and condensation of aromatic rings.[1,27–33] The increase in the aromatic sheet diameter (L_a) is also reflected in the number of aromatic rings per sheet (NO_{ar}). In the parent asphaltenes, the average number of aromatic rings per sheet is in the range of 4–8 rings, while it is around 14 in the graphene derivatives obtained at 950 °C.

To further verify the XRD findings, the average diameter of aromatic sheet has been also measured by Raman spectroscopy.

AlHumaidan and Rana[20] have recently tested and assessed different equations proposed in the literature for calculating L_a from the Raman spectra for both crystalline and amorphous carbon-based materials. Their findings indicated that the proposed correlations for measuring L_a in crystalline[34–36] and amorphous carbon[37] could not be utilized for the semi-crystalline asphaltene. AlHumaidan and Rana[15] designated that the optimum equation for measuring L_a in asphaltene is the one proposed by Tuinstra and Koenig,[38] but only when the integrated areas are used in defining I_D/I_G instead of peak intensities. Fig. 6 illustrates the L_a measurement from Raman spectra for the parent asphaltenes and their corresponding graphene derivatives. The L_a measurements for the semi-crystalline asphaltenes and their semi-crystalline carbonized products (≤600 °C) were obtained from Tunistra's empirical equation; whereas the L_a measurements for the well crystalline carbonized products (>800 °C) were performed using the equation proposed by Cancado *et al.*[34] Fig. 6 suggests comparable L_a measurements between Raman and XRD, in terms of the overall trend; however, the exact values of L_a have some variations, which are anticipated from different characterization tools.

The TEM results in Fig. 4 and 5 also confirm the expansion in L_a with carbonization. The results designate that the average L_a measurement for the asphaltenes from LF, KEC, and Ku to be around ~15 Å, ~16 Å, and ~21 Å, respectively. These measurements are in good agreement with the ones reported from the XRD and Raman. The TEM results also reveal a substantial increase in the size of L_a for the graphene derivatives obtained at 800–900 °C (L_a > 70 Å). Generally speaking, the TEM results are consistent with the XRD and Raman results, where all of them are confirming the expansion in aromatic sheet diameter during carbonization due to secondary reactions in the aromatic core.

Elimination of alkyl side-chains

The elimination of the alkyl side chains from the asphaltene molecules can be verified by different characterization
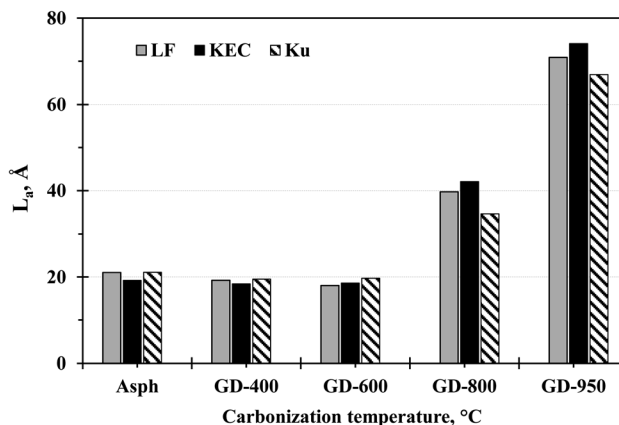

Fig. 6 Average diameter of aromatic sheet (L_a) measured by Raman spectroscopy for the parent asphaltenes and their corresponding graphene derivatives.

techniques. The XRD results confirm the side chain removal by various indicators. For instance, the observed reduction in L_c can be partially attributed to the elimination of the alkyl side chains. Furthermore, the initial reduction in L_a measurement at mild carbonization (*i.e.*, 400 °C) is another indication of side chains removal. The slight enhancement in aromatic sheet stacking at mild carbonization is also another sign of alkyl side chain removals, since these side chains normally impede the aromatic sheet from stacking. The removal of aliphatic carbon in the side chains is also clearly reflected in the XRD analysis by the notable increase in aromaticity from approximately ∼0.17 to about ∼0.80. This aromaticity was calculated from the area of resolved peaks for the γ and graphene bands; therefore, the calculated values were based on the aromatic carbon that contributed to the graphene band, rather than all aromatic carbon of asphaltene. Consequently, the aromaticity reported from XRD measurement is only indicative and could not have represented the true aromaticity.

The Raman results also confirmed the removal of the paraffinic side chains from the asphaltene molecule. This is clearly exemplified in Fig. 2 by the D-band, which become more prominent as the carbonization severity increases. Beyond 800 °C, the D-band intensity and band-width almost became comparable to that of the G-band, which could either suggest significant structural disorders or a high functionalization degree.[39] Wang *et al.*[40] observed such increase in the D-band size for co-doped graphene, and attributed it to the presence of heteroatoms (S & N) and to the increase in aromatic sheet detectable edges, which became more measurable with the removal of alkyl side chains. Maslova *et al.*[41] also reported similar D-band behaviour while carbonizing anthracene-based carbon. Maslova and coworkers associated the increase in D-band intensity and bandwidth to the secondary carbonization and to the release of hydrogen atoms that are fixed on the edges of the ploy-aromatic layers, which indicate the removal of side chains.

The TEM results also endorse the removal of side-chains during thermal treatment. The TEM images of parent asphaltene aggregates have revealed tangled structures with edges similar to cauliflower (Fig. 4). Such tangled structures are mainly caused by the presence of the alkyl-side chains, which impede the aromatic sheets from stacking.[26] The observed tangled structure nearly disappeared after thermal treatment, as shown in Fig. 5, where the stacking of the aromatic sheets became more evident due to the rapture of the paraffinic side chains.

The FTIR analysis was also employed in this study to verify the removal of side chains and to elucidate the changes in functional groups with asphaltene molecule exposure to the thermal treatment. Fig. 7 illustrates the FTIR spectra of the three asphaltenes along with their corresponding graphene derivatives. The diffused reflectance infrared transform (DRIFT) spectra of the asphaltene molecules shows profusions in saturated hydrocarbons, which are revealed in the absorption bands at 2957, 2924, 2850, 1455, and 1376 cm^{-1}.[42–44] The peaks at 2957, 2924, and 2850 cm^{-1} presents the saturated CH stretching vibrations; whereas the ones at 1455 and 1376 cm^{-1} features CH
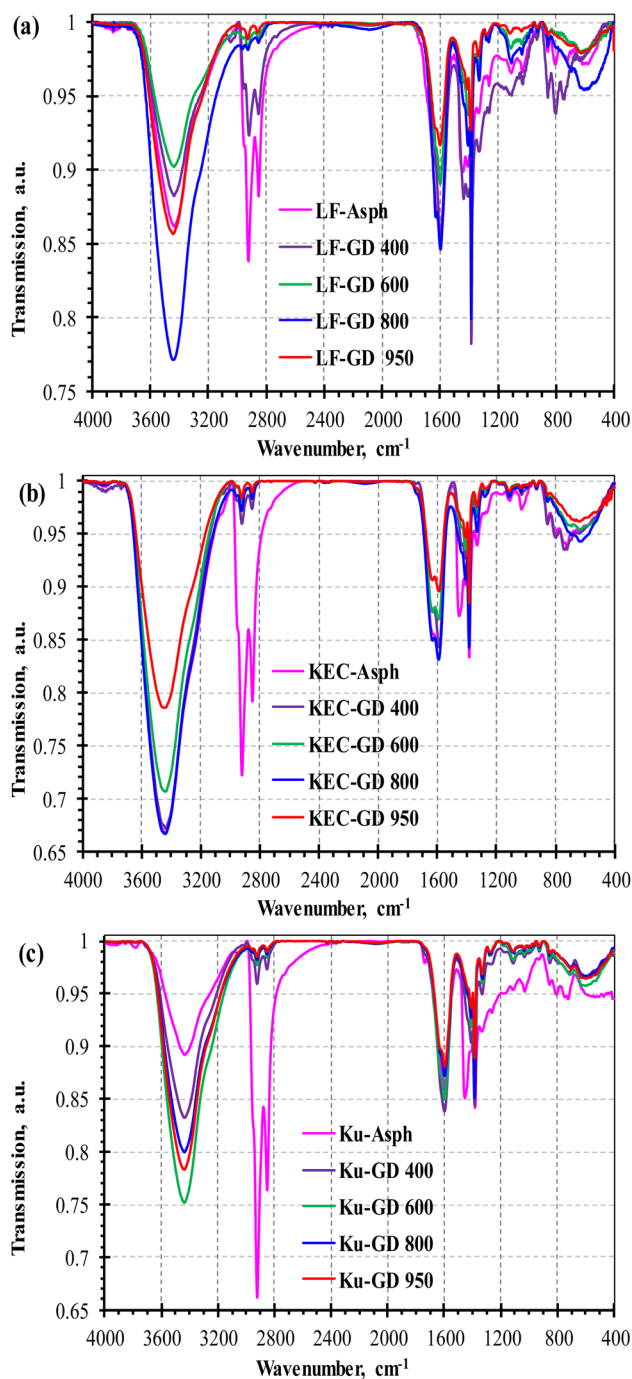

Fig. 7 DRIFT spectra of the three asphaltenes and their corresponding graphene derivatives at different temperatures: (a) LF, (b) KEC and (c) Ku.

bending vibrations. The spectra also illustrate aromatic ring (aryl) hydrocarbons at the regions of 3150–3000, 1615–1580, 1250–950, and 900–700 cm^{-1}.[42–44] The 3150–3000 cm^{-1} region is normally assigned to aromatic C–H stretching vibration, while 1250–950 cm^{-1} and 900–700 cm^{-1} are respectively ascribed to aromatic C–H in-plane bending and aromatic C–H out-of-plane bending. Conversely, the 1615–1580 cm^{-1} region is assigned to the C=C aromatic stretching.
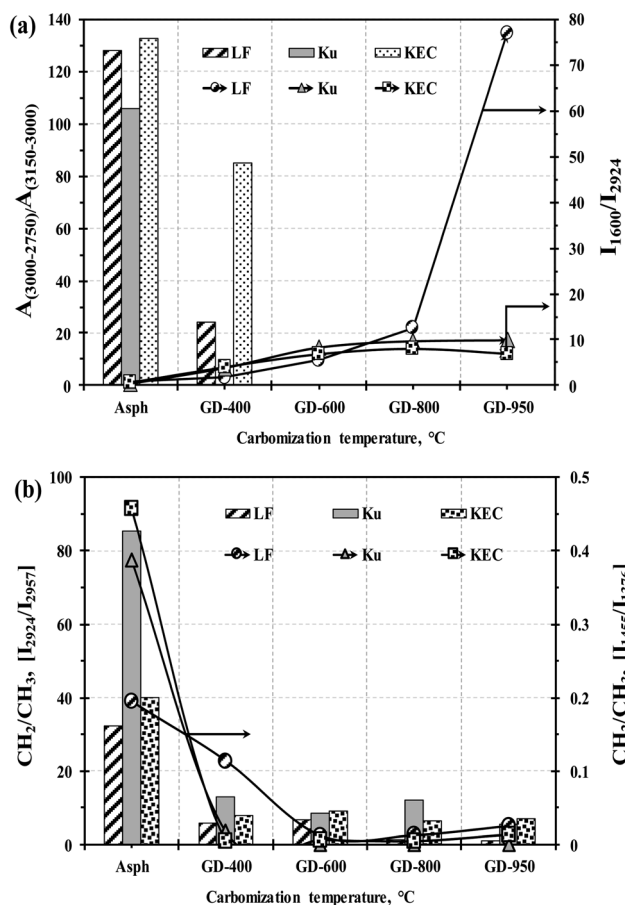
Fig. 8 Effect of thermal treatment on graphene derivatives; (a) increase in aromaticity (b) decrease in the average length of alkyl side chains.

The DRIFT spectra of the graphene derivatives, on the other hand, illustrate obvious changes when compared to their corresponding parent asphaltenes. For example, the prominent peaks of aliphatic stretching vibration in the 2850–2950 cm^{-1} region (*i.e.*, –CH$_{3(as)}$ at 2957, –CH$_{2(as)}$ at 2924, and –CH$_{2(s)}$ at 2850 cm^{-1}) have progressively reduced with the increase in carbonization temperature; indicating the removal of side chains. Similarly, the peaks of aliphatic CH bending vibration at 1455 cm^{-1} (–CH$_{2(as)}$) and 1376 cm^{-1} (–CH$_{3(s)}$) are barely observed after severe thermal treatment. Fig. 8 illustrates the impact of operating severity on graphene derivative nature. The effect of thermal treatment in product aromaticity is exemplified in Fig. 8a by monitoring the ratio between the aliphatic C–H stretching modes (3000–2750 cm^{-1}) and the aromatic C–H stretching mode (3150–3000 cm^{-1}); denoted as $A_{(3000-2750)}/A_{(3150-3000)}$. The observed reduction in the aliphatic/aromatic ratio [$n(CH_{1-3})_{al}/m(CH)_{ar}$] clearly endorses the removal of aliphatic side-chain from the large aromatic cluster of the asphaltene molecule. The increase in aromaticity with carbonization is also confirmed through the intensity ratio between C=C aromatic stretch at 1600 cm^{-1} and CH aliphatic stretch at 2924 cm^{-1}. To further confirm the removal

of aliphatic chains, the changes in aliphatic nature in the graphene derivatives have been investigated by determining the ratio between the methylene and methyl groups [CH$_2$/CH$_3$]; obtained from the intensity ratios of I_{2924}/I_{2957} and I_{1455}/I_{1376}.[42] Fig. 8b clearly illustrates significant reductions in the CH$_2$/CH$_3$ ratio with carbonization temperature, which would suggest a considerable shrinkage in the length of alkyl side chains.

Comparison between structural parameters

The comparison between the structural parameters of the three parent asphaltenes and their corresponding graphene derivatives clearly revealed significant changes. Nevertheless, some structural parameters have not been affected by the thermal treatment such as the layer distance between the aromatic sheets (d_m), which almost remained constant at all carbonization temperatures. The XRD results showed d_m to be around 3.6 Å while the TEM designated it to be in the range of 3.4–3.7 Å, which is close to the interlayer distance between planes in the base state of a multi-layer graphene (*i.e.*, 3.4 Å). Conversely, other structural parameters revealed significant variations with temperature such as the cluster diameter, the number of aromatic sheet per stack, the average diameter of aromatic sheet, the average number of aromatic rings per sheet, and the aromaticity (Fig. 9). Fig. 9 clearly indicates that graphene derivatives from different origins tend to become more comparable in structural parameters as the carbonization temperature increase, despite the obvious differences in their parent asphatlenes properties. This observation is mainly evident at 950 °C (GD-950), where the structural parameters of the different graphene derivatives almost illustrated similar values. Such finding might suggest that the transformation of asphaltene to graphene derivative by thermal treatment has an optimum temperature, which might fall in the range of 900–1000 °C. At this temperature range, the three transformation mechanisms (*i.e.*, thermal exfoliation, aromatic core secondary reactions, and alkyl side chains removals) approach their peaks. This finding might also suggest that the structural parameters of the parent asphaltenes are not of paramount importance if the thermal treatment takes place at relatively high temperatures. The similar trends observed in Fig. 9 between certain structural parameters are mainly attributed to their interrelation.[1,16,17] For example, the increase in the stack height (L_c) should be reflected in the number of aromatic sheet per stack (n), and similarly the changes in the aromatic sheet diameter (L_a) should reflect on the number of aromatic rings per sheet (NO$_{ar}$). The relations between these structural parameters are given as follows:

$$n = \frac{L_c}{d_m} + 1$$
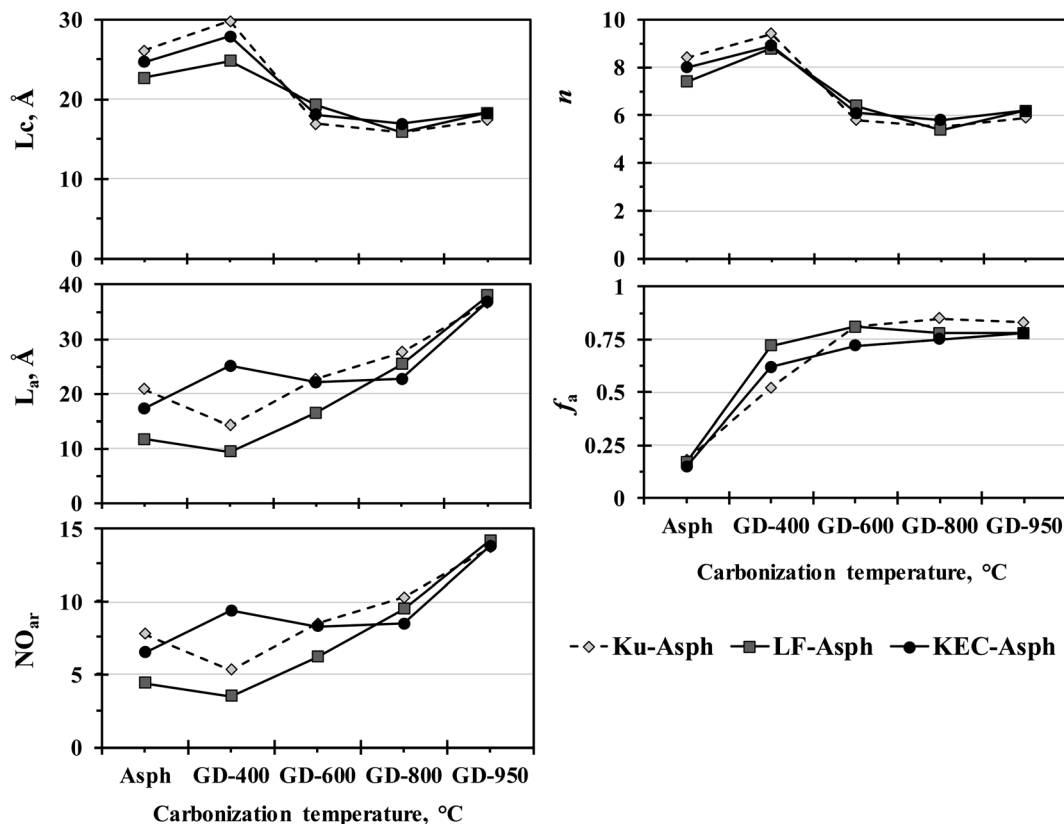
$$NO_{ar} = \frac{L_a}{2.667}$$

Fig. 9 Changes in structural parameters in graphene derivatives with temperature.

Quantification of heteroatoms

Heteroatoms in asphaltene are always associated with challenges in deep conversion processes, and their extractions require selective catalytic hydrotreatments. The presence of these heteroatoms are expected in our graphene derivatives, since the proposed carbonization process is mainly based on thermal treatment. The purities of graphene and graphene derivatives are important for many industrial applications; however, high purity is not always essential. In fact, for some industrial applications heteroatoms are introduced to graphene to enhance certain properties such as the capacitive performance, electrical conductivity, surface activity, chemical reactivity, and mechanical properties. Among the most commonly employed heteroatoms in graphene doping are nitrogen and sulfur,[45–52] and both of them naturally exist in the aliphatic and aromatic constituents of asphaltene molecules. The presence of these heteroatoms, in both asphaltene and graphene derivatives, can be clearly observed in DRIFT spectra of Fig. 7. The
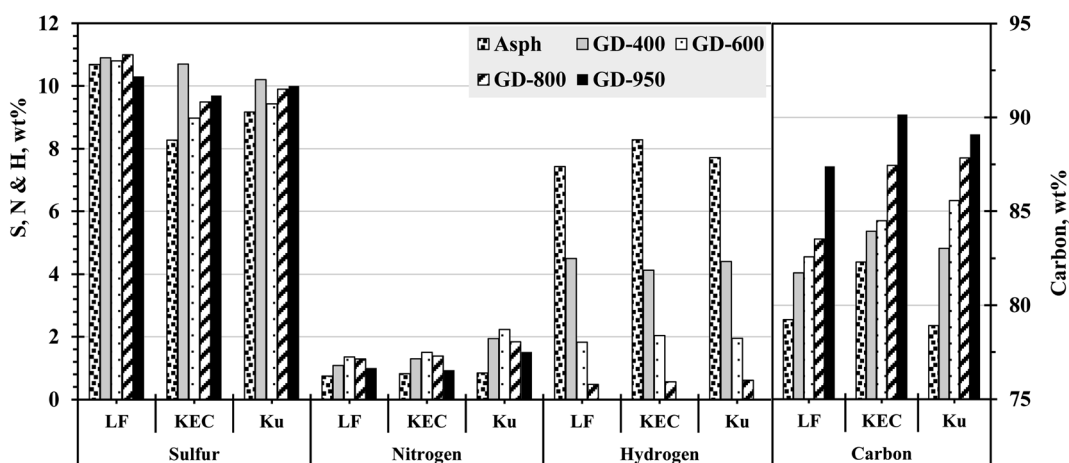

Fig. 10 Variation in elemental composition with carbonization temperature.
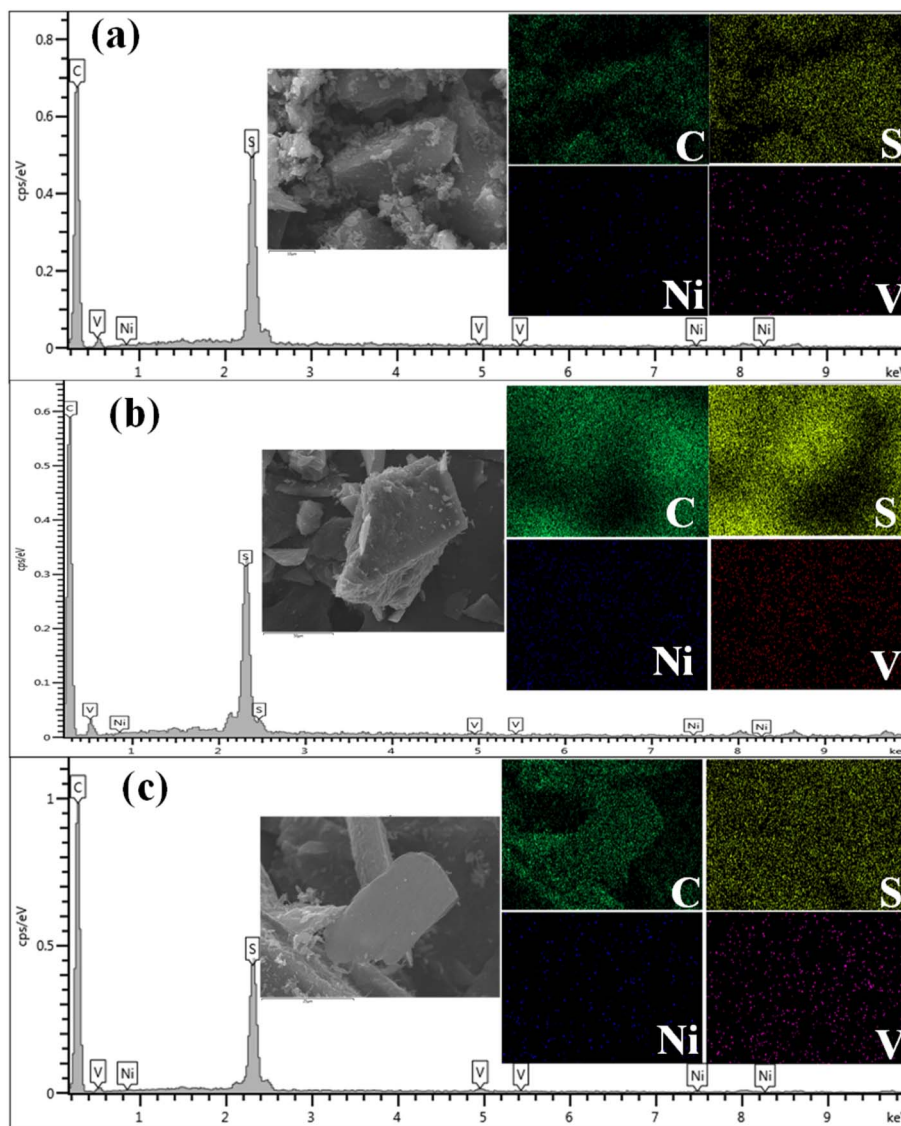
Fig. 11 SEM-EDS elemental mapping of graphene derivatives obtained at 950 °C (a) LF, (b) KEC and (c) KU.

broad bands of absorption at 1735–1640 cm^{-1} and at 1280–1000 cm^{-1} are indicative of the presence of functional groups, such as ketones, amides, and sulfoxides. The peak at 1030 cm^{-1}, which assigned S=O stretching vibration of sulfoxide, also confirmed the presence of heteroatoms and would suggest the possible oxidation of thiophenic compounds.[42,53] Furthermore, the absorption peaks at the regions of 1360–1250 cm^{-1} and 600–715 cm^{-1} are respectively assigned to the C–N stretching of aromatic amine and the C–S stretching of thioethers and disulfides.[43] The FTIR spectra of the asphaltenes also confirm the presence of several oxygen functional groups at 3450–3350 cm^{-1}, 1730–1630 cm^{-1}, and 1050–1250 cm^{-1}.[43,44] The broad band in the region of 3450–3350 cm^{-1} is ascribed to the O–H stretching vibrations, which could either be attributed to the OH from C–OH or the water adsorption.[54] On the other hand, the absorption peaks at 1730–1630 cm^{-1} are typically attributed to C=O stretching vibration of carboxyl and carbonyl functional groups. The absorption peaks at 1050–1250 cm^{-1}, conversely, are normally assigned to the C–O stretching vibrations from the epoxy groups (C–O–C) and alcohol (C–OH).

In this study, the atomic composition of the major elements in asphaltenes and their corresponding graphene derivatives have been quantified using the CHNS elemental analysis, Fig. 10. The results reveal an upsurge in the carbon contents and a reduction in the hydrogen contents as the severity of thermal treatment increased. The decrease in hydrogen content can mainly be ascribed to the removal of aliphatic substituents as previously indicated. The elemental analysis also would imply that the observed losses in hydrogen (wt%) are mainly recompensed by escalations in carbon contents, which confirm the previous conclusion about the aromatic core secondary reactions. The elemental analysis also ratifies the existence of sulfur and nitrogen. The insignificant changes in sulfur and nitrogen contents with thermal treatment would imply that

these heteroatoms are evenly distributed between the aliphatic and aromatic constituents. Consequently, the heteroatoms in the aliphatic constituents are eliminated with the removal of side chains, while the heteroatoms in the aromatic hydrocarbons should remain in the nearly intact aromatic layers. AlHumaidan et al.[27] reported similar observation while studying asphaltene behaviour in deep conversion processes, where they reported insignificant changes in sulfur and nitrogen contents after the thermal cracking of residual oil. They attributed findings to the nearly equally distributed heteroatoms between aliphatic and aromatic constituents and the difficulty associated with heteroatoms removals from the aromatic sheets without selective catalytic hydrotreatment (i.e., hydro-desulfurization and hydro-denitrogenation).

The presence of heteroatoms and metals was also qualitatively confirmed by the SEM elemental mapping. The elemental analysis by SEM-EDS is highly dependent on the examined site (i.e., irradiated zone). Therefore, the elemental composition obtained by this technique is more indicative than quantitative. In agreement with the CHNS analysis, the SEM-EDS results in

Fig. 11 confirm the presence of sulfur even after thermal treatment. Nitrogen, on the other hand, was difficult to detect in the EDS, and this is mainly attributed to their position inside the sample.[26] Fig. 11 also illustrates traces of nickel and vanadium, which naturally exist in the core of asphaltene molecules in the form of porphyrin. The removal of these metal impurities cannot be attained by thermal treatment and requires catalytic hydrotreatment, known as hydro-demetalization. Therefore, the presence of metal traces is expected in the graphene derivatives, but in the form of inorganic species since the porphyrin structure normally decomposes at high temperature.

Quantification of defect density

Defect quantification for graphene and graphene-related materials is very fundamental for determining their possible applications. Significant efforts have been made to quantify the defect and disorder in graphene-related materials.[55–57] Fig. 12 quantifies the density of defect for the different graphene derivatives by determining the average distance between two defects (L_D). The L_D measurement showed an almost constant value (i.e., $\sim$1.25 nm) for each set of samples. The constant trend in L_D measurement was seen to be consistent with the trends observed in sulfur and nitrogen measurements, which would infer that the observed defects could mainly be related to the presence of these heteroatoms in the aromatic sheets. Similar level of defect has been reported for S–N co-doped graphene by Wang et al.[47]

Conclusions

A thermal treatment method is proposed in this study to convert asphaltenes from different origins to graphene derivatives. The proposed thermal treatment method successfully transformed the asphaltene molecules to few-layer graphene derivatives by reducing the number of aromatic sheet per stack, expanding the aromatic sheet diameter, and removing the alkyl side chains from the aromatic core. The reduction in the number of aromatic sheet per stack is attributed to thermal exfoliation, while the increase in aromatic sheet diameter with temperature is credited to the secondary reactions in the aromatic core. The elimination of alkyl side chains, on the other hand, is mainly ascribed to thermal cracking. The structural parameters obtained from the different analytical techniques would confirm the formation of graphene derivative of less than 6 layers. This study also revealed that graphene derivatives from different origins tend to become very comparable in structural parameters at high carbonization temperature, regardless of the obvious differences in their parent asphaltenes structures and compositions. The quantification of heteroatoms, on the other hand, confirmed the presence of sulfur and nitrogen in the graphene derivatives and indicated insignificant changes in their contents with treatment, which would imply that these heteroatoms are evenly distributed between the intact aromatic core and the detached aliphatic side chains. The defect density has been also quantified in the parent asphaltenes and their corresponding graphene derivatives by measuring the average
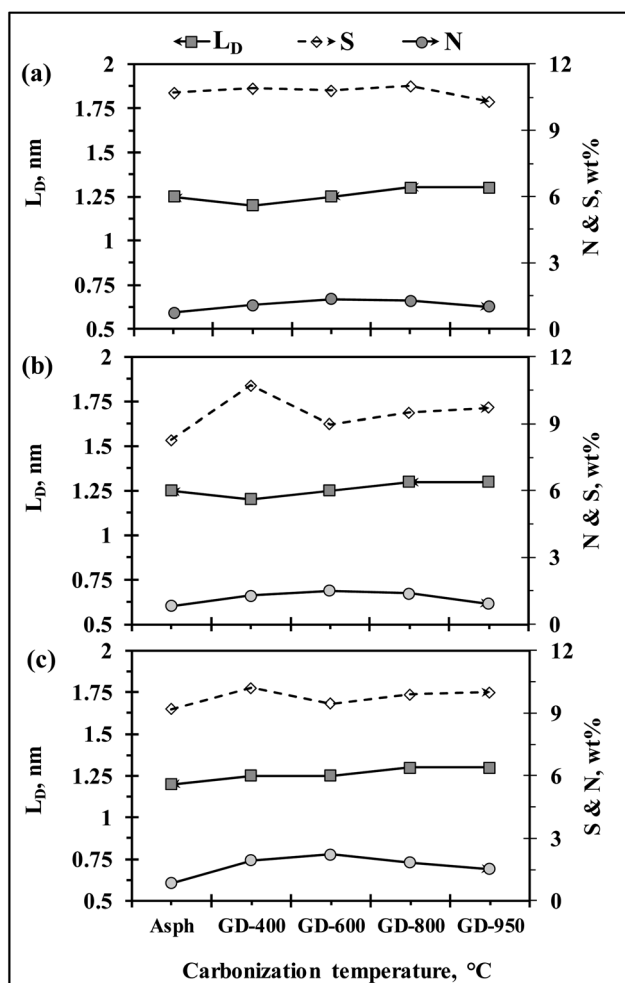

Fig. 12 Quantifications of defect densities in the three parent asphaltenes along with their corresponding graphene derivatives; (a) LF, (b) KEC and (c) Ku.

distance between defects. The consistent trends observed between defect densities and heteroatom contents in all graphene derivatives might suggest that the observed defects could mostly be related to the presence of heteroatoms.

Conflicts of interest

There are no conflicts to declare.

Acknowledgements

References

1 F. S. AlHumaidan, A. Hauser, M. S. Rana, H. M. S. Lababidi and M. Behbehani, Changes in asphaltene structure during thermal cracking of residual oils: XRD study, *Fuel*, 2015, **150**, 558.

2 I. F. Cheng, Y. Xie, R. Allen Gonzales, P. R. Brejna, J. P. Sundararajan, B. A. Fouetio Kengne, D. Eric Aston, D. N. McIlroy, J. D. Foutch and P. R. Griffiths, Synthesis of graphene paper from pyrolyzed asphalt, *Carbon*, 2011, **49**(8), 2852.

3 I. F. Cheng, Y. Xie, D. N. McIlroy, J. D. Foutch and P. R. Griffiths, *Method for making graphene*, US Pat., 2012/0228555A1, 2012.

4 Z. Liu, Z. Tu, Y. Li, F. Yang, S. Han, W. Yang, L. Zhang, G. Wang, C. Xu and J. Gao, Synthesis of three-dimensional graphene from petroleum asphalt by chemical vapor deposition, *Mater. Lett.*, 2014, **122**, 285.

5 E. M. Deemer and R. R. Chianelli, Compositions and methods related to doped graphene derived from asphaltenes, *US Pat.* 9862609B2, 2018.

6 C. Xu, G. Ning, X. Zhu, G. Wang, X. Liu, J. Gao, Q. Zhang, W. Qian and F. Wei, Synthesis of graphene from asphaltene molecules adsorbed on vermiculite layers, *Carbon*, 2013, **62**, 213.

7 X. Wu, B. Ma, Y. Xu, J. Xu, H. Zhai, Z. Xiong, X. Liao, X. Shi and X. Chen, Preparation of Three-Layer Graphene Sheets from Asphaltenes Using a Montmorillonite Template, *J. Nanomater.*, 2019, **2019**, 6.

8 O. W. Tanimola, Methods for synthesis of graphene derivatives and functional materials from asphaltenes, *US Pat.* 2016/0039678A1, 2016.

9 F. S. AlHumaidan, M. S. Rana and V. Mari. Synthesizing graphene derivatives from asphaltene, *US Pat.* 11505466B1, 2022.

10 F. S. AlHumaidan, M. S. Rana, V. Mari, N. Rajasekaran, H. Y. AlHenyyan and A. A. Ali, Synthesizing few-layer carbon materials from asphaltene by thermal treatment, *Diamond Relat. Mater.*, 2022, **129**, 109316.

11 M. Wu, J. Liao, L. Yu, R. Lv, P. Li, W. Sun, R. Tan, X. Duan, L. Zhang, F. Li and J. Kim, 2020 Roadmap on carbon materials for energy storage and conversion, *Chem.–Asian J.*, 2020, **15**(7), 995–1013.

12 J. G. Manjunatha and C. M. Hussain, *Carbon Nanomaterials-Based Sensors: Emerging Research Trends in Devices and Applications*, Elsevier, 2022.

13 H. Yu, Y. Feng, C. Chen, Z. Zhang, Y. Cai, M. Qin and W. Feng, Thermally conductive, self-healing, and elastic polyimide@ vertically aligned carbon nanotubes composite as smart thermal interface material, *Carbon*, 2021, **179**, 348–357.

14 F. Lv, M. Qin, F. Zhang, H. Yu, L. Gao, P. Lv, W. Wei, Y. Feng and W. Feng, High cross-plane thermally conductive hierarchical composite using graphene-coated vertically aligned carbon nanotubes/graphite, *Carbon*, 2019, **149**, 281–289.

15 F. S. AlHumaidan, M. S. Rana, H. M. Lababidi and A. Hauser, Pyrolysis of asphaltene derived from residual oils and their thermally treated pitch, *ACS Omega*, 2020, **5**(38), 24412.

16 T. F. Yen, J. G. Erdman and S. S. Pollack, Investigation of the structure of petroleum asphaltenes by X-ray diffraction, *Anal. Chem.*, 1961, **3**(11), 1587.

17 M. N. Siddiqui, M. F. Ali and J. Shirokoff, Use of X-ray diffraction in assessing the aging pattern of asphalt fractions, *Fuel*, 2002, **81**(1), 51–58.

18 H. L. Poh, P. Simek, Z. Sofer and M. Pumera, Sulfur-doped graphene via thermal exfoliation of graphite oxide in H_2S, SO_2, or CS_2 gas, *ACS Nano*, 2013, **7**(6), 5262–5272.

19 J. Ancheyta, F. Trejo and M. S. Rana, *Asphaltenes: Chemical Transformation during Hydroprocessing of Heavy Oils*. CRC press, Taylor & Francis Group, 2010.

20 F. S. AlHumaidan and M. S. Rana, Determination of asphaltene structural parameters by Raman spectroscopy, *J. Raman Spectrosc.*, 2021, **52**(11), 1878.

21 A. C. Ferrari, J. C. Meyer, V. Scardaci, C. Casiraghi, M. Lazzeri, F. Mauri, S. Piscanec, D. Jiang, K. S. Novoselov, S. Roth and A. K. Geim, Raman Spectrum of Graphene and Graphene Layers, *Phys. Rev. Lett.*, 2006, **97**(18), 187401.

22 A. Gupta, G. Chen, P. Joshi, S. Tadigadapa and P. C. Eklund, Raman Scattering from High-Frequency Phonons in Supported n-Graphene Layer Films, *Nano Lett.*, 2006, **6**(12), 2667.

23 D. Graf, F. Molitor, K. Ensslin, C. Stampfer, A. Jungen, C. Hierold and L. Wirtz, Spatially Resolved Raman Spectroscopy of Single- and Few-Layer Graphene, *Nano Lett.*, 2007, **7**(2), 238.

24 Z. Ni, Y. Wang, T. Yu and Z. Shen, Raman spectroscopy and imaging of graphene, *Nano Res.*, 2008, **1**(4), 273.

25 H. Wang, Y. Wang, X. Cao, M. Feng and G. Lan, Vibrational properties of graphene and graphene layers, *J. Raman Spectrosc.*, 2009, **40**(12), 1791.

26 F. S. AlHumaidan, M. S. Rana, N. J. Tanoli, H. M. S. Lababidi and N. A. AlNajdi, Changes in asphaltene surface topography with thermal treatment, *Arabian J. Chem.*, 2020, **13**, 5377.

27 F. S. AlHumaidan, A. Hauser, M. S. Rana and H. M. S. Lababidi, NMR characterization of asphaltene derived from residual oils and their thermal decomposition, *Energy Fuels*, 2017, **31**, 3812.

28 A. Peraza, M. Sanchez and F. Ruette, Modeling free-radical reactions, produced by hydrocarbon cracking, with asphaltenes, *Energy Fuels*, 2010, **24**, 3990.

29 T. Takatsuka, S. Inoue and Y. Hori, Role of asphaltene cracking in bottom conversion, *Petroleum Technology Quarterly*, Spring, 1999, pp. 61–67.

30 P. E. Savage, M. T. Klein and S. G. Kukes, Asphaltene reaction pathways, 1. Thermolysis, *Ind. Eng. Chem. Process Des. Dev.*, 1985, **24**(4), 1169.

31 P. E. Savage and M. T. Klein, Asphaltene reaction pathways. 2. Pyrolysis of n-pentadecylbenzene, *Ind. Eng. Chem. Res.*, 1987, **26**(3), 488.

32 P. E. Savage, M. T. Klein and S. G. Kukes, Asphaltene reaction pathways. 3. Effect of reaction environment, *Energy Fuels*, 1988, **2**(5), 619.

33 P. E. Savage and M. T. Klein, Asphaltene reaction pathways-V. Chemical and mathematical modeling, *Chem. Eng. Sci.*, 1989, **44**(2), 393.

34 L. G. Cancado, K. Takai, T. Enoki, M. Endo, Y. A. Kim, H. Mizusaki, A. Jorio, L. N. Coelho, R. Magalhaes-Paniago and M. A. Pimenta, General equation for the determination of the crystallite size La of nanographite by Raman spectroscopy, *Appl. Phys. Lett.*, 2006, **88**, 163106.

35 O. A. Maslova, M. R. Ammar, G. Guimbretiere, J. N. Rouzaud and P. Simon, Determination of crystallite size in polished graphitized carbon by Raman spectroscopy, *Phys. Rev. B: Condens. Matter Mater. Phys.*, 2012, **86**(13), 134205.

36 P. Mallet-Ladeira, P. Puech, C. Toulouse, M. Cazayous, N. Ratel-Ramond, P. Weisbecker, G. R. L. Vignoles and M. Monthioux, A Raman study to obtain crystallite size of carbon materials: a better alternative to the Tuinstra–Koenig law, *Carbon*, 2014, **80**, 629.

37 A. C. Ferrari and J. Robertson, Interpretation of Raman spectra of disordered and amorphous carbon, *Phys. Rev. B: Condens. Matter Mater. Phys.*, 2000, **61**(20), 14095.

38 F. Tuinstra and J. L. Koenig, Raman Spectrum of Graphite, *J. Chem. Phys.*, 1970, **53**, 1126.

39 P. L. Yap, S. Kabiri, D. N. Tran and D. Losic, Multifunctional binding chemistry on modified graphene composite for selective and highly efficient adsorption of mercury, *ACS Appl. Mater. Interfaces*, 2019, **11**(6), 6350.

40 T. Wang, L. X. Wang, D. L. Wu, W. Xia and D. Z. Jia, Interaction between nitrogen and sulfur in co-doped graphene and synergetic effect in supercapacitor, *Sci. Rep.*, 2015, **5**(1), 1.

41 O. A. Maslova, M. R. Ammar, C. Fantini, S. A. Barannikova and M. A. Pimenta, Resonant Raman scattering of anthracene-based carbons in the secondary carbonization stage, *J. Raman Spectrosc.*, 2021, **52**(3), 670.

42 F. S. AlHumaidan, A. Hauser, M. S. Rana and H. M. S. Lababidi, Impact of thermal treatment on Asphaltene functional groups, *Energy Fuels*, 2016, **30**, 2892.

43 J. Coates, Interpretation of Infrared Spectra, A Practical Approach, in *Encyclopedia of Analytical Chemistry*, John Wiley & Sons Ltd, Chichester, 2000, pp. 1–23.

44 V. Tucureanu, A. Matei and A. M. Avram, FTIR Spectroscopy for Carbon Family Study, *Crit. Rev. Anal. Chem.*, 2016, **46**(6), 502.

45 H. Wang, T. Maiyalagan and X. Wang, Review on Recent Progress in Nitrogen-Doped Graphene: Synthesis, Characterization, and Its Potential Applications, *ACS Catal.*, 2012, **2**(5), 781.

46 Y. Yamada, J. Kim, S. Matsuo and S. Sato, Nitrogen-containing graphene analyzed by X-ray photoelectron spectroscopy, *Carbon*, 2014, **70**, 59.

47 T. Wang, L. X. Wang, D. L. Wu, W. Xia and D. Z. Jia, Interaction between Nitrogen and Sulfur in Co-Doped Graphene and Synergetic Effect in Supercapacitor, *Sci. Rep.*, 2015, **5**(1), 9591.

48 J. Liang, Y. Jiao, M. Jaroniec and S. Z. Qiao, Sulfur and nitrogen dual-doped mesoporous graphene electrocatalyst for oxygen reduction with synergistically enhanced performance, *Angew. Chem., Int. Ed.*, 2012, **51**, 11496.

49 X. Wang, J. Wang, D. Wang, S. Dou, Z. Ma, J. Wu, L. Tao, A. Shen, C. Ouyang, Q. Liu and S. Wang, One-pot synthesis of nitrogen and sulfur co-doped graphene as efficient metal-free electrocatalysts for the oxygen reduction reaction, *Chem. Commun.*, 2014, **50**(37), 4839–4842.

50 D. Qu, M. Zheng, P. Du, Y. Zhou, L. Zhang, D. Li, H. Tan, Z. Zhao, Z. Xie and Z. Sun, Highly luminescent S, N co-doped graphene quantum dots with broad visible absorption bands for visible light photocatalysts, *Nanoscale*, 2013, **5**(24), 12272–12277.

51 J. X. Xu, G. F. Dong, C. H. Jin, M. H. Huang and L. H. Guan, Sulfur and nitrogen co-doped, few-layered graphene oxide as a highly efficient electrocatalyst for the oxygen-reduction reaction, *ChemSusChem*, 2013, **6**, 493–499.

52 Y. Su, Y. Zhang, X. Zhuang, S. Li, D. Wu, F. Zhang and X. Feng, Low-temperature synthesis of nitrogen/sulfur co-doped three-dimensional graphene frameworks as efficient metal-free electrocatalyst for oxygen reduction reaction, *Carbon*, 2013, **62**, 296–301.

53 J. C. Poveda, D. Molina, H. Martínez, O. Florez and B. Campillo, Molecular Changes in Asphaltenes within H_2 Plasma, *Energy Fuels*, 2014, **28**(2), 735–744.

54 R. Yu, X. Zhu, J. Hu, W. Zhao and C. Fang, Preparation of graphene oxide and its modification effect on base asphalt, *Fullerenes, Nanotubes, Carbon Nanostruct.*, 2019, **27**, 256–264.

55 L. G. Cancado, A. Jorio, E. H. M. Ferreira, F. Stavale, C. A. Achete, R. B. Capaz, M. V. O. Moutinho, A. Lombardo, T. S. Kulmala and A. C. Ferrari, Quantifying Defects in Graphene via Raman Spectroscopy at Different Excitation Energies, *Nano Lett.*, 2011, **11**(8), 3190–3196.

56 S. Eigler, C. Dotzer and A. Hirsch, Visualization of defect in reduced graphene oxide, *Carbon*, 2012, **50**, 3666–3673.

57 D. Zhan and Z. Shen, Raman and Infrared Spectroscopic Characterization of Graphene, *Two-dimensional carbon: Fundamental Properties, Synthesis, Characterization, and Applications*, ed. W. Yihong; Z. Shen and T. Yu, CRC Press, 2014.